Journal of Science and Technology in Civil Engineering, HUCE, 2023, 17 (3): 102–113

AN INNOVATIVE MODEL TO ESTIMATE THE TENSION FIELD INCLINATION CONSIDERING CRACK GROWTH FOR STEEL PLATE SHEAR WALL

Chung Nguyen Van[a,*], Ali Ghamari[b]

[a]*Faculty of Civil Engineering, Ho Chi Minh City University of Technology and Education, 1 Vo Van Ngan Street, Thu Duc City, Ho Chi Minh, Vietnam*
[b]*Department of Civil Eng, Ilam branch, Islamic Azad University, Ilam, Iran*

Article history:
Received 16/02/2023, Revised 25/5/2023, Accepted 05/6/2023

Abstract

The Steel Plate Shear Walls (SPSWs) are known as a capable system to use in steel structures due to their significant advantages. Despite extensive studies concerning this system, few researchers have scrutinized the crack effect on SPSW behavior. However, the crack dramatically affected the experimental results. In the current paper, the effect of central and edge cracks, therefore, has been studied in jointed plates at mid-height of SPSW. Results indicated that the central crack is more destructive than the edge crack. The central crack having a long initial length also makes a sudden wall fracture in the elastic zone and consequently cannot be used in high seismic regions. Due to the dependence of the wall on the diagonal tension field and its angle, an equation is proposed taking into account shear, axial, and moment actions in columns, axial and moment actions in beams, as well as shear and axial actions in the plate which conform to finite element results. Because of the complication of the stress intensity factor for mode I and mode II calculations, this confidence is derived and offered.

Keywords: steel plate shear walls; crack effect; pushover curve; fracture; modification factor.

https://doi.org/10.31814/stce.huce2023-17(3)-08

1. Introduction

The experience regarding the performance of the Steel Plate Shear Walls (SPSWs) under past earthquakes and its comprehensive studies reported by researchers have encouraged the constructors to use this system in their practical projects [1]. Provided that the system is properly detailed, it will behave as a ductile system with high energy dissipation capacity [2]. Accordingly, the SPSWs can be considered capable and cost-effective systems. Ductile performance, low weight, architectural aspects, high initial stiffness, economic aspects, and no complicity in the construction of the system [3] have persuaded designers and constructors to utilize this system in practical projects.

Concerning the common stories' height in general buildings as well as shop limitations, full plates without patches are rarely utilized. But, generally, a whole/full plate without any patches has been used in experimental studies[4–8]. In practical projects, as shown in Fig. 1, separate plates assembled by welded or bolted to make an infill plate of SPSW are employed.

It is worth mentioning that the SPSWs' testing is performed with stricter than real project conditions. Also, owing to the low thickness of the infill plate made it susceptible to cracks located in the vicinity of the joints of infill plates that are prevented in lab conditions. Naturally, crack is more expected in the real condition of construction projects. Besides, reviewing previous experimental studies on SPSW [8–10] indicates that the presence of cracks is inevitable even in controlled lab conditions.

*Corresponding author. *E-mail address:* chungnv@hcmute.edu.vn (Chung, N. V.)

Although the crack affects the results of experimental tests, its effect has not been studied comprehensively until now. In other words, despite the impact of the crack on the SPSW performance, there are only two published findings considering the SPSW affected by crack [11, 12]. The crack propagation had only been numerically evaluated in these references, and the results had focused on seismic parameters of cracked SPSWs. The results showed that the crack propagated dramatically affected the structural parameters. In doing so, the present paper is supposed to deal numerically and parametrically with the effect of probable crack at mid-height of SPSW between jointed infill plates to estimate inclination field angle, to calculate stress intensity factor for mode I (KI), mode II (KII), and to recognize critical cracks.

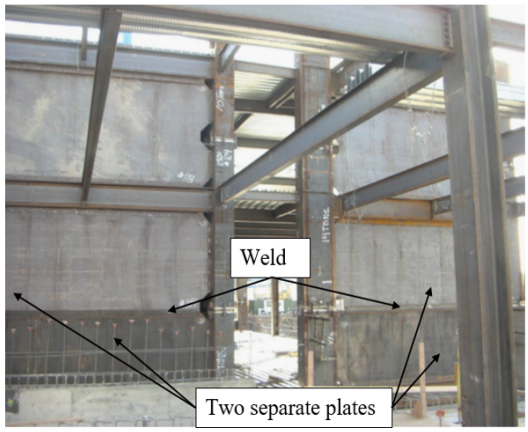

Figure 1. A schematic view of SPSW during construction

Despite limited research concerning SPSWs involved with cracks, lots of comprehensive reports have been published about the influence of the cracks on the bare plates outside of the structural system. Sih and co-workers [13] considered the pre-buckling of the cracked plate in the linear zone under axial loads (tension and compression). They revealed that increasing the crack length dwindles the elastic capacity of the cracked plate. Parallel to this research, other features of the cracked plate have been studied numerically; the influence of crack on thin panels under shear loading [14], axial compression [15], and axial tension [16]. Some researchers have investigated the crack and its propagation. In doing so, the effect of crack on dynamic analysis [17], and the method of crack propagation simulation [18, 19] have been investigated, and aspects of crack propagation in those researches have been proposed. Due to limited results reported on the crack effect on SPSWs, in this paper, the behavior of SPSWs regarding the crack effect is examined parametrically and numerically.

2. Methodology

In the present study, the behavior of SPSW considering a crack located at mid-height of SPSWs between two infill plates is numerically and parametrically investigated. As mentioned before, the infill plate of SPSWs usually consists of two separate plates joined together by welding; therefore, the formation of cracks at the mid-height of SPSWs is probable and deniable. Therefore, central and edge cracks, as displayed in Fig. 2, are analyzed to consider the effect of cracks on the SPSWs' behavior. Since the modification factor, R, is an important seismic parameter for each structure, the R factor of SPSWs with the aforementioned cracks is discussed to reveal critical cracks. The R factor is often

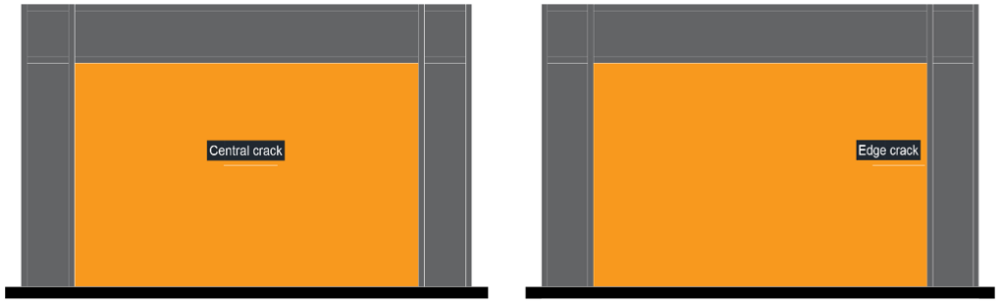

Figure 2. Schematic view of the location of the cracked plate shear walls

described as a product of several factors. Also, since the linear and nonlinear behavior of SPSWs depends upon the inclination tensile stress angle, the parametrical study is performed to propose the inclination tensile stress angle considering the crack effect.

3. Parametrically study

3.1. The inclination of tension field stress

The AISC and other Codes have proposed Eq. (1) to estimate the angle of inclination of the tension field of an SPSW:

$$\tan\alpha = \sqrt[4]{\frac{1+\dfrac{tL}{2A_C}}{1+ht\left[\dfrac{1}{A_b}+\dfrac{h^3}{360I_cL}\right]}} \tag{1}$$

where A_b and A_c are area sections of the beam and column, respectively, and I_c is the column's moment of inertia. Also, L and h are defined as the length and height of the story.

Eq. (1) has been driven using the virtual work theory whereas the effect of column shear stress, as well as the effect of the cracks, have been neglected. Then researchers [4] utilized a modified relation based on the plate girder theory for SPSWs. The proposed equation by Kulak was established based on internal works of the beam's axial force infill plate's axial force, and bending moment in columns. Since huge columns are used for SPSWs, the effect of shear stress on the columns of the SPSWs system is inevitable. Therefore, in the present paper, a new equation is presented for tension field action considering shear stress in columns and the crack effect on the infill plate.

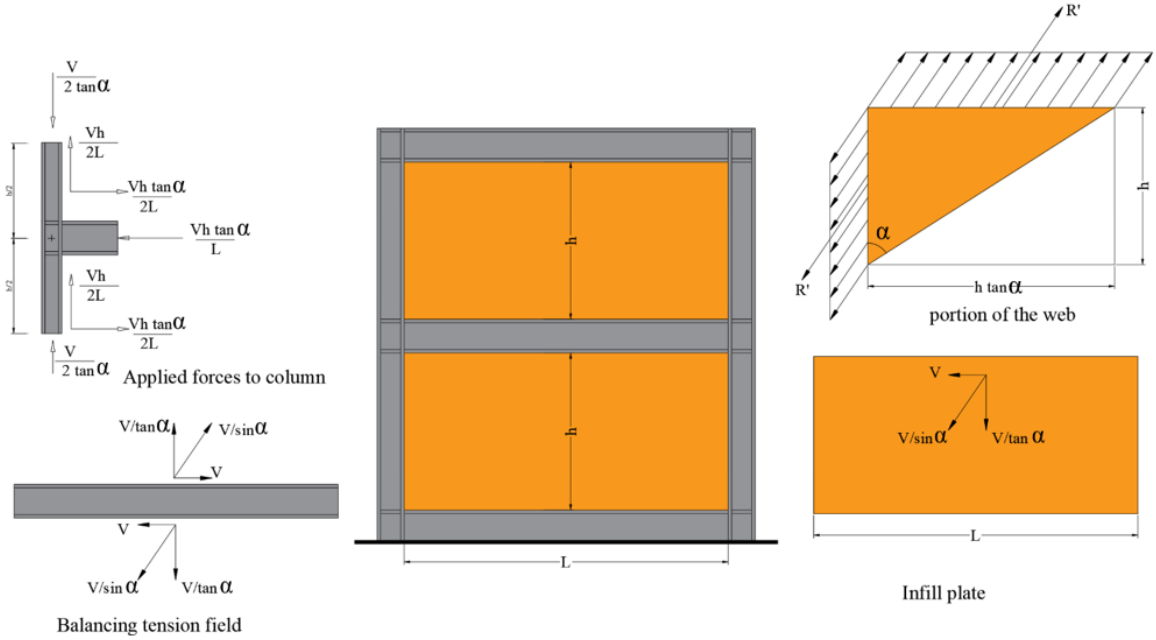

Figure 3. Free-Body diagram

Recognizing that the horizontal resistance V is only a component of the tension field created in the plate, other components of the force triangle can be calculated, as shown in Fig. 3(a). The notation α, which is used for the angle of inclination of the tension field within the web, will be constant. Thus, the vertical component of the tension field force is equally divided between the two columns. Because

the thickness of the infill plate of SPSW in two adjacent stories is equal or there is a little difference between them, interior beams are assumed to be equal, see Fig. 3(b). Based on the figure, the axial force in the beam is zero, and also internal work of shear force and bending moment will be zero (or almost zero).

The researchers assume when the crack is propagated, a portion of the plate does not contribute to resisting lateral load. What is shown in Fig. 3(d) is a portion of the web with a depth equal to the column height, h. The inclined force on the beam, as shown in Fig. 3(b), can be expressed in terms of force per unit length $V/L\sin\alpha$. Thus the total force along the horizontal portion of the web identified in Fig. 3(c) is:

$$R' = \frac{V}{L\sin\alpha}h\tan\alpha = \frac{Vh}{L\cos\alpha} \tag{2}$$

Note that no forces are shown along with the diagonal act. Since this cut is coincident with the direction of principal stress, shear stresses are zero. The work contributed by the compressive stress is assumed to be negligible compared to other terms. Therefore, no compressive force is shown along with the cut. Because the vertical portion of the web shown in Fig. 3(c) must be anchored by the column, force R' also acts on the column. Its horizontal component is $R'\sin\alpha = \frac{Vh\tan\alpha}{L}$, and its vertical component is $R'\cos\alpha = \frac{Vh}{L}$.

A free-body diagram of the left-hand column is shown in Fig. 3(d). It extends from the mid-height of one panel to the mid-height of another. The horizontal forces create the axial force in the beam. that is taken as constant at the value $\frac{Vh\tan\alpha}{L}$ as in detail it has a linearly varying shape. If we assume the column has two ends fixed supported, the mid-height moment of the column is $\frac{Vh^2\tan\alpha}{24L}$.

For an SPSW, the internal work of the system includes the contributions of the infill plate and boundary frame:

$$W_{tot} = \underset{Axial,Shear}{W_{Web}} + \underset{Axial}{W_{Beam}} + \underset{Axial,Shear,Bending}{W_{Column}} \tag{3}$$

The resulting expression for contribution to the works is:

$$W_{C_{Axial}} = \frac{V^2h}{4E.A_C\tan^2\alpha} \tag{4}$$

Also, assuming $\vartheta = 0.3$ and shear modulus equals $0.8E$, the internal shear work of the column can be presented as:

$$W_{C_{shear}} = \frac{V^2h^3\tan^2\alpha}{2\times 0.8L^2EA_{wC}} \tag{5}$$

The moment distribution in the column which is parabolic can be expressed as: $M_C = \frac{V\tan\alpha}{12L}(6hx - h^2 - 6x^2)$. Substitution and integration over both columns for internal work due to moment yields:

$$W = \int_L \frac{M^2}{2EI}dx = \frac{V^2h^5\tan 2\alpha}{720EI_cL^2} \tag{6}$$

In addition, the internal work of the beam owing to axial force is:

$$W_{B_{Axial}} = \frac{V^2h^2\tan^2\alpha}{2LEA_b} \tag{7}$$

Moreover, the internal work of the plate due to axial force and shear force is:

$$W_{Plate,Axial} = \frac{V^2 h}{2tEL_w \cos^2\alpha \sin^2\alpha} \tag{8}$$

$$W_{Plate,Shear} = \frac{V^2 h}{2 \times 0.8EtL_w \sin^2\alpha} \tag{9}$$

The total work expression then is the summation of Eqs. (2) through (9).

$$\begin{aligned} W_{tot} = {} & \frac{V^2 h}{4EA_C \tan^2\alpha} + \frac{V^2 h^3 \tan^2\alpha}{2 \times 0.8L^2 EA_{wC}} + \frac{V^2 h^5 \tan^2\alpha}{720EI_c L^2} + \frac{V^2 h^2 \tan^2\alpha}{2LEA_b} \\ & + \frac{V^2 h}{2tEL\cos^2\alpha \sin^2\alpha} + \frac{V^2 h}{2 \times 0.8EtL \sin^2\alpha} \end{aligned} \tag{10}$$

Accordingly, the equation is summarized as:

$$\tan\alpha = \sqrt[4]{\frac{2.25 + \dfrac{tL}{2A_C}}{1 + ht\left[\dfrac{1}{A_b} + \dfrac{0.625h}{A_{Wc}L} + \dfrac{h^3}{360I_c L}\right]}} \tag{11}$$

3.2. The stress field in the vicinity of the crack tip

According to the fracture mechanic theory, the crack tip stress field is formulated in Eq. (12).

$$\begin{aligned} \sigma_{xx(r,\theta)} &= \frac{KI}{\sqrt{2\pi r}} \cos\frac{\theta}{2}\left[1 - \sin\frac{\theta}{2}\sin\frac{3\theta}{2}\right] - \frac{KII}{\sqrt{2\pi r}} \sin\frac{\theta}{2}\left[2 + \cos\frac{\theta}{2}\cos\frac{3\theta}{2}\right] \\ \sigma_{yy(r,\theta)} &= \frac{KI}{\sqrt{2\pi r}} \cos\frac{\theta}{2}\left[1 + \sin\frac{\theta}{2}\sin\frac{3\theta}{2}\right] - \frac{KII}{\sqrt{2\pi r}} \sin\frac{\theta}{2}\cos\frac{\theta}{2}\cos\frac{3\theta}{2} \\ \sigma_{xy(r,\theta)} &= \frac{KI}{\sqrt{2\pi r}} \cos\frac{\theta}{2}\sin\frac{\theta}{2}\cos\frac{3\theta}{2} + \frac{KII}{\sqrt{2\pi r}} \sin\frac{\theta}{2}\left[2 + \sin\frac{\theta}{2}\sin\frac{3\theta}{2}\right] \end{aligned} \tag{12}$$

Where parameters in this equation were defined before. The *KI* is obtained according to the classical theory of fracture mechanics for in-plane shear and bending loading [14].

3.3. Numerical study

a. Material properties and loading

In this study, the A36 steel was used where the yield strength, modulus of elasticity, and Poisson's ratio of the steel is respectively 235 MPa, 210 GPa, and 0.3. Also, its fracture toughness is greater 150 MPa $\sqrt{m}$. Lateral loads are applied to the FE models up to achieving the ultimate drift angle. The ultimate drift is considered to equal 2.5% according to the ASCE 7-10 [20].

b. Verification of numerical results

In this paper, ANSYS software [21] is utilized to model and analyze the FE models. To validate the FE results, their results are compared with an experimental test reported in Ref. [4]. The geometry and mechanical properties of the FE modeling were used the same as the experimental test. As shown in Fig. 4, there is a good agreement between the test results [4] and the finite element results and for the load-displacement curves.

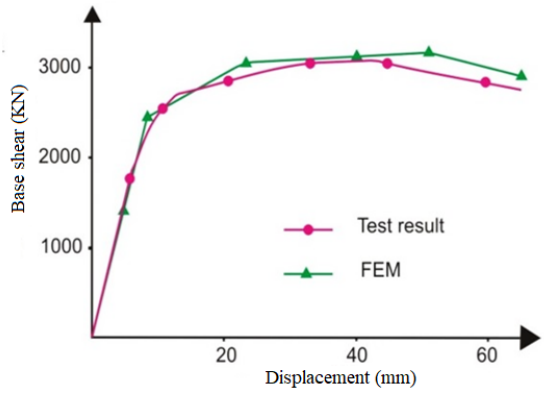

Figure 4. Comparison of FE results with experimental test

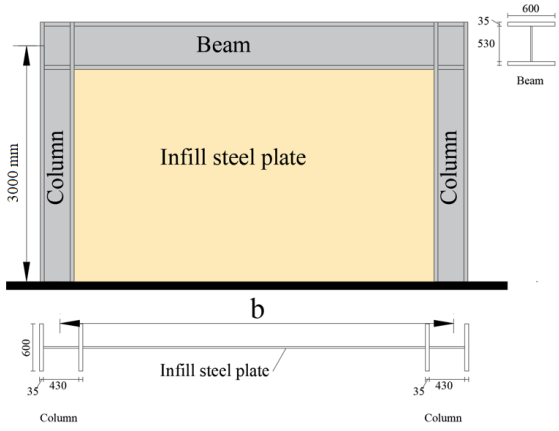

Figure 5. Geometry of finite element models (all dimensions are in mm)

c. Numerical models

To assess the accuracy of the proposed method, numerical analyses, Table 1, are performed. In doing so, The model's name contains two parts, a character and one number. The first part, character CF or EF, represents the location of the crack as a central or edge crack, respectively. The number in the second part stands for the length of the initial crack. In all of the models, the steel plate has a thickness and length of 7 mm and 4 m, respectively. The surrounding frame of the infill plate was designed according to the AISC provisions [22], and its geometric properties are presented in Fig. 5.

Table 1. The numerical models

Model	The initial crack length (mm)	The initial crack length divided by infill plate length (%)
CF-4	4	0.1
CF-8	8	0.2
CF-16	16	0.4
CF-32	32	0.8
CF-64	64	1.6
CF-128	128	3.2
CF-256	256	6.4
CF-512	512	12.8
CF-1024	1024	25.6
EF-4	4	0.1
EF-8	8	0.2
EF-16	16	0.4
EF-32	32	0.8
EF-64	64	1.6
EF-128	128	3.2
EF-256	256	6.4
EF-512	512	12.8
EF-1024	1024	25.6

4. Results and discussions

4.1. Load-displacement curve

The Load-displacement curve of FE models is plotted in Fig. 6. Referring to the figures, although the central crack has a considerable effect on the behavior of the wall, the edge cracks do have an ignorable effect. The walls with central cracks more than 128 mm in length are ruptured suddenly, and also walls with longer do not experience the nonlinear phase. The structural parameters related to the crack's location are investigated in the next parts.

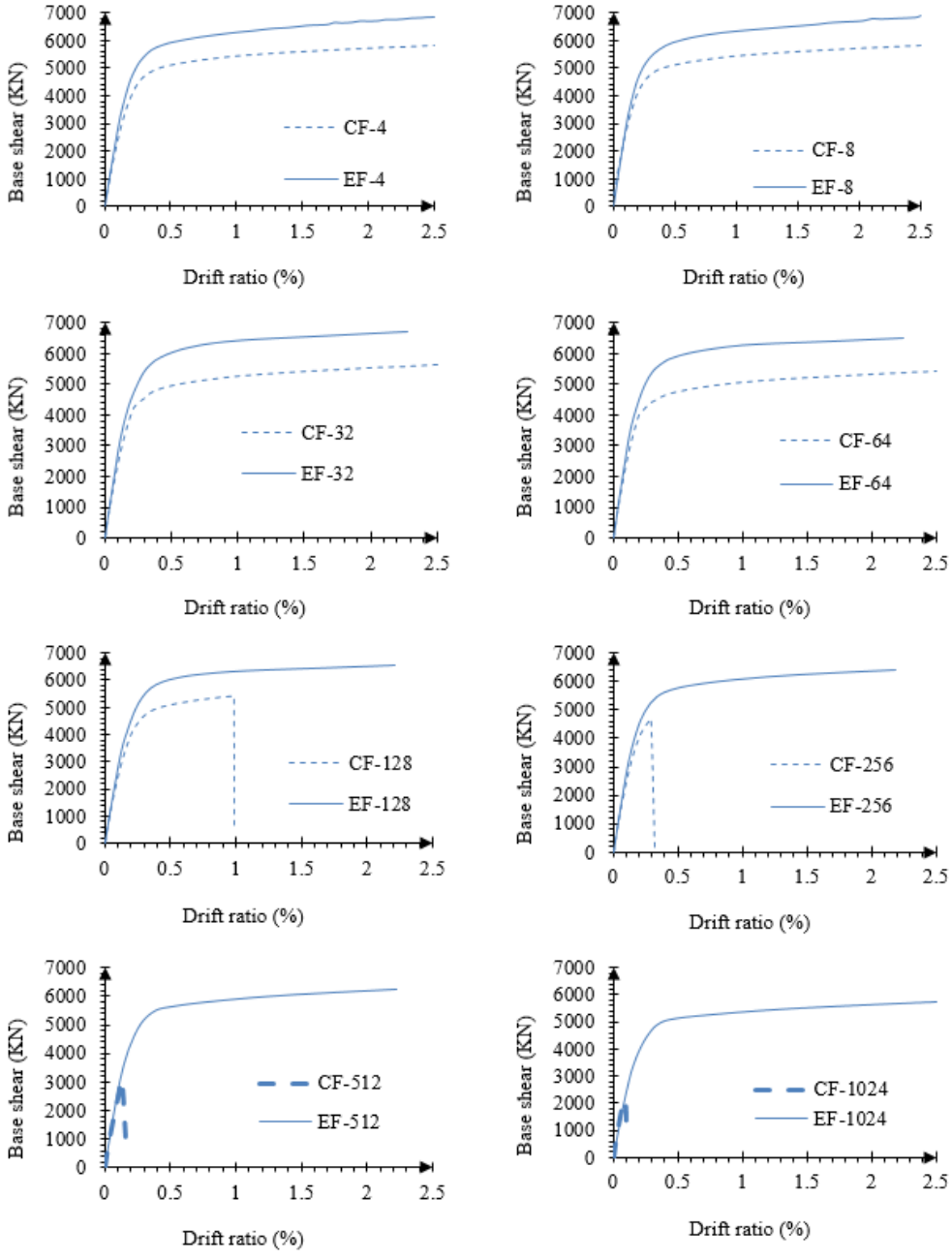

Figure 6. Load-displacement curves

4.2. The state of hinge formation in cracked walls

Figs. 7 and 8 show the state of the infill plate yielding for two crack types. According to these figures, the cracks (central and edge cracks) do not have a considerable effect on the inclination of yielding in the infill plate. It is noted that in walls with long initial cracks, the yielding starts at the crack rather than the infill plate. Increasing the initial crack length prevents tension field action from occurring. An incomplete tension field has occurred in walls with crack lengths equal to 32 mm, whereas in longer crack lengths, no tension field action occurs. Nevertheless, in walls with edge cracks, increasing initial crack length causes plastic hinges to be formed in columns instead of infill plates. In the vicinity of the crack, a portion of the infill plate does not contribute to resisting lateral loads that should be included in the SPSW design.

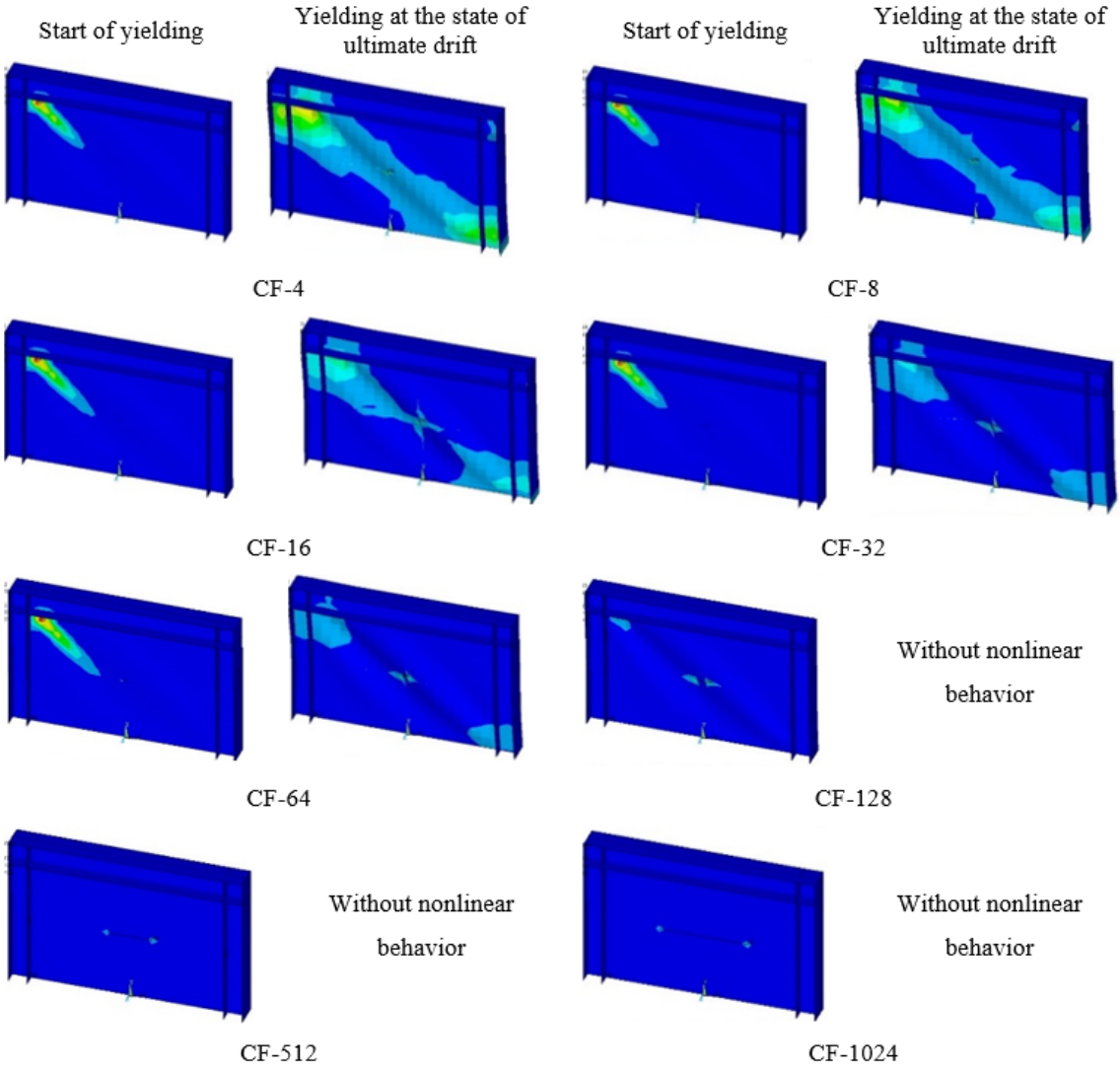

Figure 7. The state of yielding in the wall with central cracks

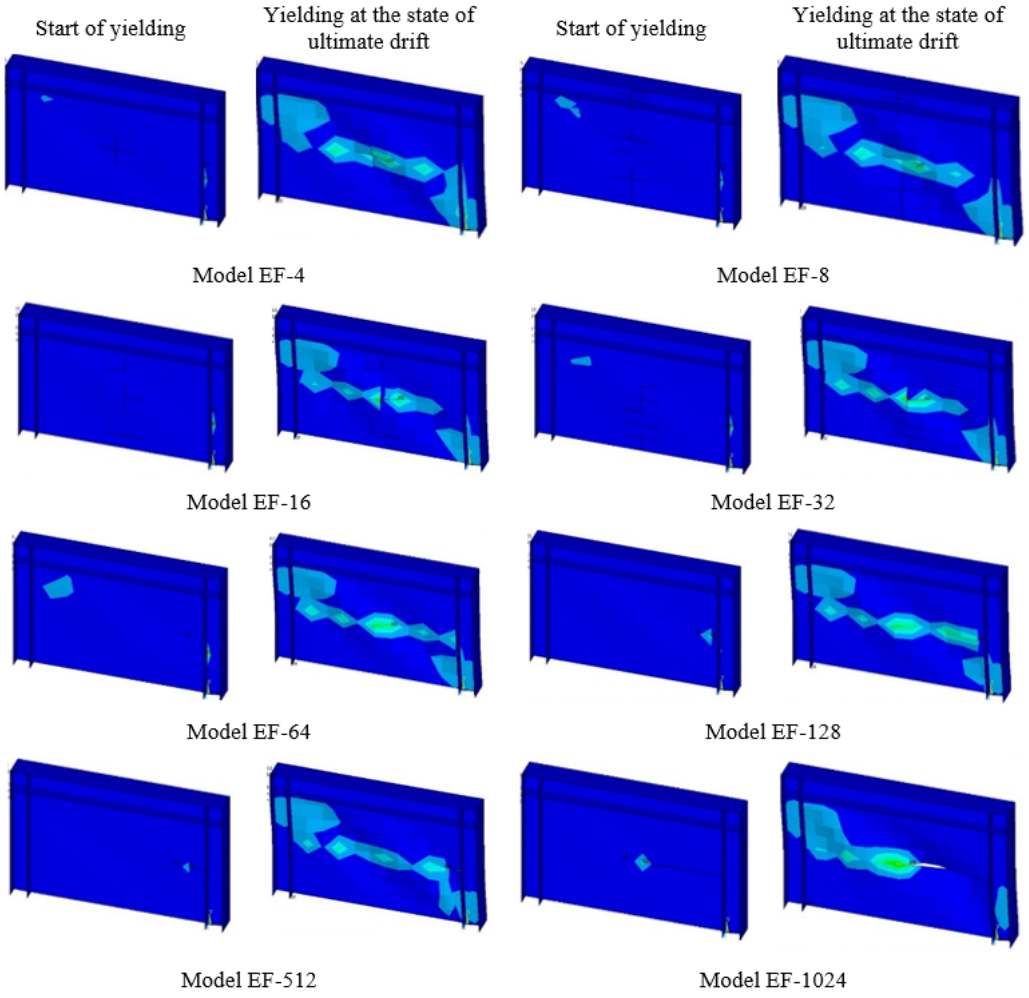

Figure 8. The state of yielding in the wall with edge cracks

4.3. Response modification factor

To assess the structural parameters, the real lateral response is generally idealized as a bilinear curve [5, 20]. According to the simplification, the modification factor, R_u, is defined as:

$$R_u = \frac{V_e}{V_s} = \frac{V_e}{V_y} \times \frac{V_y}{V_s} = R_\mu \Omega_0 \tag{13}$$

where the V_e and V_s are, respectively, the base shear corresponding to elastic behavior and the first hinge formation in the structure. Moreover, the R_μ is the period-dependent ductility factor that is equal to the ultimate elastic base shear (V_e) divided by the maximum base shear (V_y). Also, the Ω_0 is the o-verstrength factor that is equal to V_y divided by the design base shear (V_s). V_s corresponds to the first yield of the structural elements causing softness in the real envelope curve of the system.

The response modification factors calculated from the load-displacement curves of each wall are listed in Table 2. It shows that with a crack length of 4 mm or 8 mm, the cracked steel shear walls can be employed in high seismic risk areas with suitable ductile behavior expectations. But, the walls with central cracks length greater than 10% of the infill plate should be employed only in low seismic risk

areas. Since walls with longer cracks do not experience nonlinear phases (limited to elastic zones), they cannot be accounted as a suitable system against seismic excitation.

Table 2. The structural parameters of the walls include central cracks

Models	μ	R_μ	Ω_0	R_u
CF-4	9.72	4.18	2.23	7.41
CF-8	9.72	4.18	2.23	7.41
CF-16	9.72	4.22	1.89	6.33
CF-32	9.72	4.20	1.87	6.22
CF-64	9.72	4.19	1.84	6.10
CF-128	9.72	2.71	2.18	4.70
CF-256	1.45	1.35	3.07	3.29
CF-512		Elastic behavior		
CF-1024		Elastic behavior		
EF-4	9.72	4.23	2.12	8.95
EF-8	9.72	4.16	2.12	8.81
EF-16	9.72	4.2	2.09	8.77
EF-32	9.72	4.27	2.09	8.91
EF-64	9.72	4.24	2.04	8.65
EF-128	9.72	4.22	2.04	8.6
EF-256	9.72	4.18	2.07	8.65
EF-512	9.72	4.21	2.09	8.77
EF-1024	9.72	4.19	2.09	8.77

5. Accuracy of the proposed equation with FE results

Comparing the results listed in Table 3 indicates that the proposed relation has an error of less than 0.5%, while the AISC relation has more errors. This equation can be utilized for all types of cracked and uncracked SPSWs. If the crack on SPSW dines, the proposed relation and AISC relation will have almost close results.

Table 3. Verification of proposed equations

Model	Numerical	AISC	Proposed equations error percentage	AISC Error Percentage	Proposed equations
CF-4	44.52	43.52	2.47	2.25	45.62
CF-8	44.65	43.52	2.17	2.53	45.62
CF-16	45.03	43.52	1.31	3.35	45.62
CF-32	45.1	43.52	1.15	3.5	45.62
CF-64	45.62	43.52	0	4.6	45.62
CF-128	45.74	43.52	0.26	4.85	45.62
CF-256	45.85	43.52	0.5	5.08	45.62
CF-512	45.9	43.52	0.61	5.19	45.62
CF-1024	45.75	43.52	0.28	4.87	45.62
EF-4	45.77	43.52	0.33	4.92	45.62
EF-8	45.85	43.52	0.5	5.08	45.62

Model	Numerical	AISC	Proposed equations error percentage	AISC Error Percentage	Proposed equations
EF-16	45.9	43.52	0.61	5.19	45.62
EF-32	46.01	43.52	0.85	5.41	45.62
EF-64	45.62	43.52	0	4.6	45.62
EF-128	45.85	43.52	0.5	5.08	45.62
EF-256	45.9	43.52	0.61	5.19	45.62
EF-512	46.2	43.52	1.26	5.8	45.62

6. Conclusions

In the present paper, the impact of the crack, central and edge, located at mid-height of SPSWs between two plates on the behavior of SPSW was investigated, and the following results are briefly concluded:

- Central cracks are more serious than edge cracks in the SPSW systems. These are due to the failure of SPSW with the central crack despite edge cracks and their contained R factor.

- Walls with central crack lengths longer than 128 mm and 512 mm were ruptured and they did experience low energy absorption and without nonlinear zone. This means that the wall with such a crack cannot be measured as a ductile system.

- The state of the infill plate yielding for two crack types shows that the cracks (central and edge cracks) do not have a considerable effect on the inclination of yielding in the infill plate. Also, increasing the initial crack length prevents tension field action from occurring.

- In walls with long initial cracks, the yielding starts at the crack instead of the infill plate. An incomplete tension field has occurred in walls with crack lengths equal to 32 mm, whereas in longer crack lengths, no tension field action occurs. In the vicinity of the crack, a portion of the infill plate does not contribute to resisting lateral loads that should be accounted for in the design of SPSW.

- Walls containing central cracks with a length of nearly 10% of the wall plate can be used only in low seismic risk areas and with low ductility expectations. For bigger cracks, the wall cannot be regarded as a load-bearing seismic system since its behavior is limited to the elastic region.

- However, cracks with a length of less than 25% of the wall length have little influence on the ductility factor and overstrength factor. A slight decrease in response modification factor is derived from the edge cracks. Edge cracks with a length of 1024mm lead to a reduction in energy absorption by 18% when compared to the wall without cracks. This reduction is much less than the one due to a central crack with the same length.

- Comparing the results of the proposed relation to estimating the inclination tension angle with finite element results indicates that the proposed relation has an error of less than 0.5%.

Acknowledgement

This work belongs to the project in 2024 funded by Ho Chi Minh City University of Technology and Education, Vietnam.

References

[1] Shishkin, J. J., Driver, R. G., Grondin, G. Y. (2009). Analysis of steel plate shear walls using the modified strip model. *Journal of Structural Engineering*, 135(11):1357–1366.

[2] Astaneh-Asl, A. (2001). *Seismic behavior and design of steel shear walls*. Structural Steel Educational Council Moraga, CA.

[3] Khaloo, A., Foroutani, M., Ghamari, A. (2019). Influence of diagonal stiffeners on the response of steel plate shear walls (SPSWs) considering crack propagation. *Bulletin of Earthquake Engineering*, 17(9): 5291–5312.

[4] Driver, R. G., Kulak, G. L., Kennedy, D. J. L., Elwi, A. E. (1998). Cyclic test of four-story steel plate shear wall. *Journal of Structural Engineering*, 124(2):112–120.

[5] Toduţ, C., Dan, D., Stoian, V., Fofiu, M. (2023). Theoretical and experimental study of damaged reinforced concrete shear walls strengthened with FRP composites. *Composite Structures*, 313:116912.

[6] Wu, Y., Fan, S., Guo, Y., Duan, S., Wu, Q. (2023). Experimental study and numerical simulation on the seismic behavior of diagonally stiffened stainless steel plate shear walls under low cyclic loading. *Thin-Walled Structures*, 182:110165.

[7] Zhou, L., Tan, P., Teng, X. (2023). Experiment and analysis of self-centering semicircular corrugated steel plate shear walls with edge stiffeners. *Journal of Building Engineering*, 66:105876.

[8] Xu, Z., Chen, Z., Dong, X., Zuo, Y. (2023). Experimental study on seismic behavior of lightweight concrete-filled cold-formed steel shear walls strengthened using horizontal reinforcement. *Journal of Earthquake Engineering*, 1–35.

[9] Guendel, M., Hoffmeister, B., Feldmann, M. (2011). Experimental and numerical investigations on steel shear walls for seismic retrofitting. In *Proceedings of the 8th International Conference on Structural Dynamics*, 474–481.

[10] Alavi, E., Nateghi, F. (2013). Experimental study of diagonally stiffened steel plate shear walls. *Journal of Structural Engineering*, 139(11):1795–1811.

[11] Broujerdian, V., Ghamari, A., Ghadami, A. (2016). An investigation into crack and its growth on the seismic behavior of steel shear walls. *Thin-Walled Structures*, 101:205–212.

[12] Shayanfar, M., Broujerdian, V., Ghamari, A. (2019). Numerically and parametrically investigating the cracked steel plate shear walls (SPSWs). *Iranian Journal of Science and Technology, Transactions of Civil Engineering*, 44(2):481–500.

[13] Sih, G. C., Lee, Y. D. (1986). Tensile and compressive buckling of plates weakened by cracks. *Theoretical and Applied Fracture Mechanics*, 6(2):129–138.

[14] Dong, J., Ma, X., Zhuge, Y., Mills, J. E. (2018). Unilateral contact buckling behaviour of orthotropic plates subjected to combined in-plane shear and bending. *International Journal of Solids and Structures*, 150:135–153.

[15] Bert, C. W., Devarakonda, K. K. (2003). Buckling of rectangular plates subjected to nonlinearly distributed in-plane loading. *International Journal of Solids and Structures*, 40(16):4097–4106.

[16] Khedmati, M. R., Edalat, P., Javidruzi, M. (2009). Sensitivity analysis of the elastic buckling of cracked plate elements under axial compression. *Thin-Walled Structures*, 47(5):522–536.

[17] Ebrahimi, M. T., Dini, D., Balint, D. S., Sutton, A. P., Ozbayraktar, S. (2018). Discrete crack dynamics: A planar model of crack propagation and crack-inclusion interactions in brittle materials. *International Journal of Solids and Structures*, 152-153:12–27.

[18] Kroon, M. (2014). Energy release rates in rubber during dynamic crack propagation. *International Journal of Solids and Structures*, 51(25-26):4419–4426.

[19] Tho, P. D., Tien, T. M., Thanh, D. T., Ngan, V. M., Ngoc, V. M., Sorelli, L. (2022). Experimental investigation of the secondary creep of fiber reinforced concrete at high stress: Macroscopic measurement and digital image correlation. *Journal of Science and Technology in Civil Engineering (STCE) - HUCE*, 16(1):19–28.

[20] ASCE (2010). *Minimum design loads for buildings and other structures*. ASCE 7-10, Reston, VA.

[21] ANSYS (2016). *User Manual*. ANSYS, Inc., Canonsburg, PA.

[22] AISC (2007). *Steel design guide 20, steel plate shear walls*. Chicago (IL): American Institute of Steel Cons.